

Article

Application of $Zn_{1-x}Cd_xS$ Photocatalyst for Degradation of 2-CP and TC, Catalytic Mechanism

Jingxin Tan ¹, Guoqiang Wei ², Zhen Wang ², Hui Su ¹, Lingtao Liu ¹, Chunhu Li ¹ and Junjie Bian ^{1,*}

¹ Key Laboratory of Marine Chemistry Theory and Technology of Ministry of Education, Ocean University of China, Qingdao 266100, China

² Shandong Haijingtian Environmental Technology Corporation, Binzhou 256600, China

* Correspondence: junjiebian@ouc.edu.cn; Tel.: +86-(532)-66782502

Abstract: $Zn_{1-x}Cd_xS$ catalysts with Zeolitic Imidazolate Framework-8 (ZIF-8) as the precursor were successfully prepared by ion exchange method, and the ability and electrochemical properties of a series of ZIF-8, ZnS and $Zn_{1-x}Cd_xS$ catalysts in photocatalytic degradation of 2-CP and TC were investigated. Doping of Cd ions was able to modulate the ZnS band gap width and improve the utilization of visible light by the photocatalyst. The nanocage catalysts with hollow structure of $Zn_{1-x}Cd_xS$ have better photocatalytic response. The removal of photocatalytic pollutants was up to 90% under optimal conditions. Using a Peroxymonosulfate (PMS)-assisted system to improve the degradation efficiency of 2-chlorophenol and tetracycline hydrochloride under visible light, we present a possible mechanism of $Zn_{1-x}Cd_xS$ as a photocatalyst for degradation in persistent pollutants and in PMS-assisted photocatalysis. Four active species, O_2^- , h^+ , $-OH$, and $SO_4^{\bullet-}$, can be generated to degrade 2-chlorophenol and tetracycline hydrochloride under PMS-assisted activation. $Zn_{1-x}Cd_xS$ nanocage with high activity and stability provides a feasible approach to catalytically remove persistent pollutants from aqueous solutions under visible light conditions.

Keywords: nanocage photocatalyst; $Zn_{1-x}Cd_xS$; 2-CP; TC; PMS; degradation



Citation: Tan, J.; Wei, G.; Wang, Z.; Su, H.; Liu, L.; Li, C.; Bian, J.

Application of $Zn_{1-x}Cd_xS$ Photocatalyst for Degradation of 2-CP and TC, Catalytic Mechanism. *Catalysts* **2022**, *12*, 1100. <https://doi.org/10.3390/catal12101100>

Academic Editor: Didier Robert

Received: 18 August 2022

Accepted: 21 September 2022

Published: 23 September 2022

Publisher's Note: MDPI stays neutral with regard to jurisdictional claims in published maps and institutional affiliations.



Copyright: © 2022 by the authors. Licensee MDPI, Basel, Switzerland. This article is an open access article distributed under the terms and conditions of the Creative Commons Attribution (CC BY) license (<https://creativecommons.org/licenses/by/4.0/>).

1. Introduction

With the development of the world economy and the production and abuse of pesticides, deodorants, and antibiotic drugs being discharged into the environment, a large number of organic pollutants has been causing environmental pollution and water pollution [1]. These pollutants mainly include antibiotics (e.g., tetracycline hydrochloride, ciprofloxacin [2], etc.), chlorophenols (e.g., 2-chlorophenol, 4-chlorophenol, etc.), etc. Tetracycline hydrochloride [3,4], as an antibiotic that can be widely used, is often applied to prevent infections. Excessive use can cause resistance to microorganisms in the water and cause incalculable harm to the environment [5,6]. In contrast, 2-chlorophenol pollution is caused by the misuse of pesticides and other insecticides, which can cause incalculable harm to human health and daily life [7,8]. The removal of pollutants from water bodies has become an urgent issue at this stage.

At present, the treatment of pollutants in wastewater has been a great challenge. The most commonly used methods for the wastewater treatment containing pollutants are photocatalytic degradation [9], ion exchange [10], and adsorption [11,12]. Photocatalytic technology can convert pollutants in water into CO_2 and H_2O based on the rational use of visible light, without secondary pollution. A green, energy-saving and effective operation can effectively alleviate environmental pollution and the energy crisis [13,14]. However, the removal of pollutants by photocatalysis alone is more limited, and the removal of pollutants from water bodies by PMS-assisted photocatalysis [15,16]. This is due to the synergistic effect of photocatalysis and PMS on the activation of the photocatalyst and thus on the degradation in organic pollutants. PMS is able to capture photogenerated electrons, thus

prolonging the complexation of electrons and catalyst, as well as increasing the efficiency of photocatalysis [17,18].

The core of photocatalysis is searching for a suitable and high performing catalyst [19]. Metal sulfides are widely used in photocatalysis due to their suitable band structure [20–22]. ZnS is an n-type semiconductor, which is widely used, simple and easy to be prepared, and has a high electron mobility [23,24]. Due to the band gap limitation of ZnS, it only responds well to UV light [25]. CdS has high visible light utilization [26,27]. Reddy et al. [28] synthesized CdS-ZnS core-shell nanoparticles by a two-step method, which expanded the surface area of the catalyst, increased the active sites of the catalyst, and significantly improved the degradation efficiency of MO. Liu et al. [29] synthesized ZnCdS solid solution by precipitation hydrothermal method, which has a suitable band gap compared with ZnS, can improve the utilization of visible light to a certain extent, and can separate free electrons and holes while preventing their complexation.

Metal–organic frameworks (MOFs) materials are porous materials composed of organic ligands and inorganic ions, which have gradually become the focus of scientists' research, mainly due to their high specific surface area, high porosity and easy modification [30–32]. MOFs materials with hollow nanostructures can facilitate electron-hole migration, and thus have been widely studied. Chen et al. [33] successfully prepared ZnCdS hollow nanoframeworks with ZIF-8 as precursor, which greatly improved the separation and transfer of carriers and had superior performance in the field of photocatalytic hydrogen production. Bai et al. [34] synthesized $Zn_{1-x}Cd_xS$ /CdS heterojunctions via a low-temperature sulfidation method to effectively drive hydrogen production. Lin et al. [35] synthesized rhombic dodecahedral $Cd_{0.5}Zn_{0.5}S$ that demonstrated the removal ability of organic pollutants.

In this paper, we have successfully prepared hollow nano $Zn_{1-x}Cd_xS$ materials by a two-step sulfidation and cation exchange method, using ZIF-8 as precursor, and investigated the removal of pollutants 2-CP and TC from water under visible light irradiation conditions, as well as under PMS-assisted conditions. Through a combination of capture experiments and kinetic fitting, we speculated on the possible reaction mechanism. This led us to propose a new method for the removal of pollutants from water.

2. Results and Discussion

2.1. Characterization of the Synthesized $Zn_{1-x}Cd_xS$

As can be seen in Figure 1a, the synthesized $Zn_{1-x}Cd_xS$ catalyst with ZIF-8 as the precursor has a very distinctive dodecahedral structure with an average particle size of 800 nm. The SEM images of $Zn_{1-x}Cd_xS$ from Figure 1c,d show that the dodecahedral structure of the ZIF-8 precursor did not change significantly after sulphidation and Cd doping. The SEM images of the ZIF-8 precursors showed that the dodecahedral structure did not change significantly after sulphidation and Cd doping, but a clear hollow structure was formed inside. The modification of the ZIF-8 precursor did not destroy the complete dodecahedral structure and retained the prismatic frame. The elemental distribution of $Zn_{1-x}Cd_xS$ is also shown in Figure 1e, where the elements Zn, Cd and S are uniformly distributed in the catalyst. In Figure 2 the SEM images were analysed using image analysis software and a certain amount of particles were selected to measure their average initial size, giving an average particle size of approximately 800 nm for the $Zn_{1-x}Cd_xS$ catalyst.

In this work, ZIF-8 was synthesized according to the method reported in the literature by standing at room temperature, and according to the XRD image Figure 3a, the synthesized ZIF-8 has obvious diffraction peaks and a more consistent structure with the simulated ZIF-8, indicating the successful preparation of ZIF-8 crystals with high crystallinity. The X-ray diffraction pattern after ion exchange is shown in Figure 3b, where the position of the diffraction peak on the (1,1,1) crystal plane is gradually shifted to a lower angle as the doping of Cd^{2+} increases, indicating that the introduction of Cd^{2+} is not a simple physical mixing, but is introduced into the ZnS lattice.

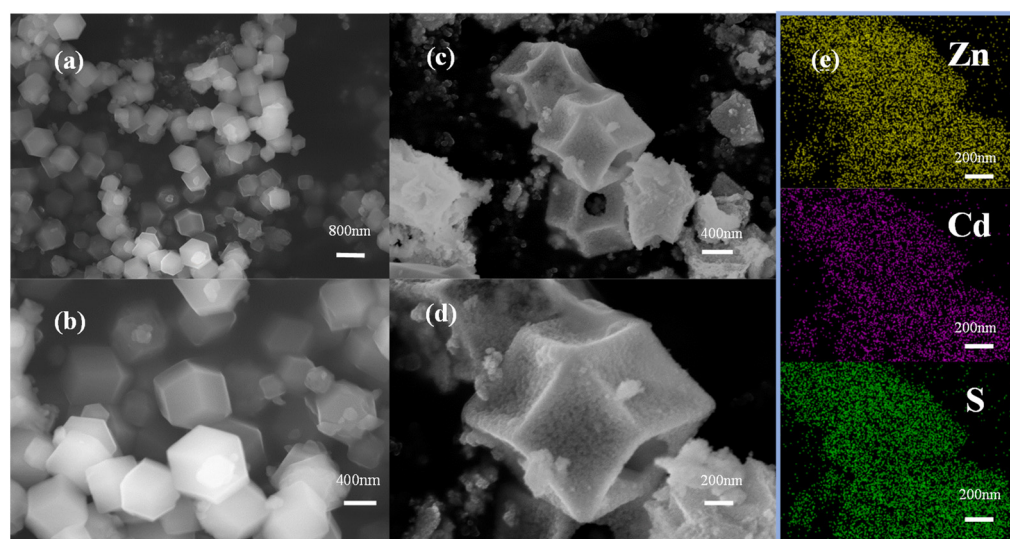


Figure 1. (a,b) SEM images of ZIF-8; (c,d) SEM images of $Zn_{1-x}Cd_xS$; (e) corresponding EDS mapping of $Zn_{1-x}Cd_xS$.

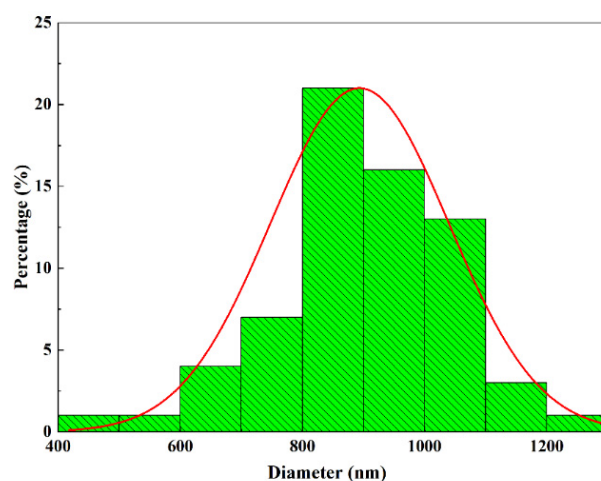


Figure 2. Particle size distribution of prepared $Zn_{1-x}Cd_xS$ catalyst.

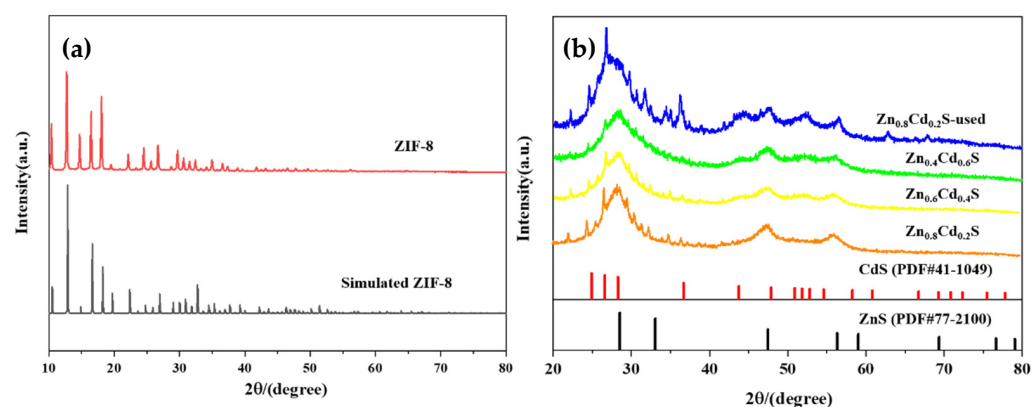


Figure 3. XRD of (a) ZIF-8 and ZnS, and (b) different metal ratios of $Zn_{1-x}Cd_xS$.

The light absorption performance determines the light utilization and catalytic activity of the photocatalyst. The light absorption properties of ZnS and $Zn_{0.8}Cd_{0.2}S$ were investigated using UV-vis diffuse reflectance spectroscopy (UV-vis DRS). According to Figure 4, the ZnS catalyst with ZIF-8 catalyst as precursor has a strong absorption peak at 360 nm,

which is consistent with what was previously reported [36]. The visible light absorption of $\text{Zn}_{0.8}\text{Cd}_{0.2}\text{S}$ is enhanced due to the introduction of Cd^{2+} . The bandgap energy (E_g) of the catalyst can be calculated by the Kubelka–Munk method using the $\alpha(h\nu) = A(h\nu - E_g)^{n/2}$, where α , h , ν and A denote the absorption coefficient, Planck's constant, optical frequency and constant, respectively [37]. The calculation shows that the bandgap energy of ZnS is 3.60 eV, while that of $\text{Zn}_{0.8}\text{Cd}_{0.2}\text{S}$ is 2.88 eV.

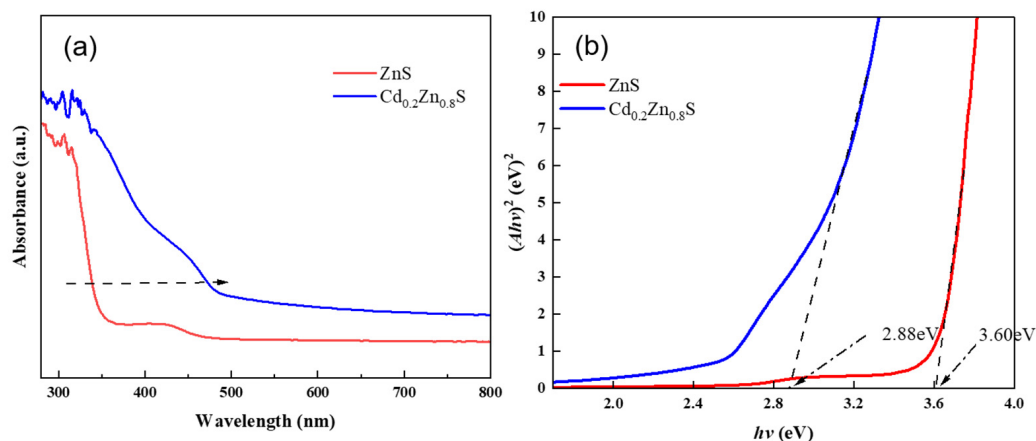


Figure 4. (a) UV-vis DRS of ZnS and $\text{Zn}_{0.8}\text{Cd}_{0.2}\text{S}$ (b) Plot of transformed Kubelka-Munk function versus photon energy for ZnS and $\text{Zn}_{0.8}\text{Cd}_{0.2}\text{S}$.

The N_2 adsorption–desorption isotherms were used to analyze the specific surface area, pore volume and pore size distribution of the samples. It can be seen that the catalysts all exhibit a similar shape to the Type I isotherms. The specific surface areas of ZIF-8, ZnS and $\text{Zn}_{0.8}\text{Cd}_{0.2}\text{S}$ measured by the Barrett–Joyner–Halenda (BJH) method were 1035.7082 m^2/g , 261.6770 m^2/g and 576.2332 m^2/g , respectively, and the pore volumes were 0.4900 cm^3/g , 0.2816 cm^3/g , 0.1160 cm^3/g . The larger specific surface area and pore volume of $\text{Zn}_{0.8}\text{Cd}_{0.2}\text{S}$ compared to ZnS is due to the larger ionic radius of Cd^{2+} compared to Zn^{2+} , which is caused by the ion exchange [33]. Both the increase in specific surface area and pore volume facilitate increased adsorption of pollutant molecules, thus promoting photocatalytic degradation reactions.

2.2. Photocatalytic Performance of Photocatalysts

The performance of the catalysts was assessed by their effectiveness in removing persistent pollutants from aqueous solutions. Then, 2-CP (50 mg/L) was removed from aqueous solutions with an initial pH of six using catalysts containing different Cd contents. The experimental results in Figure 5a show that light irradiation has little effect on the degradation in 2-CP when no catalyst is added. The best degradation effect of 90% was achieved with the addition of a catalyst with a Cd doping ratio of 20% under the same experimental conditions. In contrast, the adsorption effect of the catalyst on pollutants decreases with the increase in the amount of Cd introduced into the catalyst. The aqueous solution containing the contaminant TC (40 mg/L) was removed by $\text{Zn}_{1-x}\text{Cd}_x\text{S}$ catalysts with different Cd-containing ratios at an initial pH = 6. The experimental results Figure 5b show that without the addition of $\text{Zn}_{1-x}\text{Cd}_x\text{S}$ catalyst the removal efficiency for TC is almost zero, while with the addition of catalyst the best degradation can reach 87%. This indicates that the $\text{Zn}_{1-x}\text{Cd}_x\text{S}$ catalyst has a high efficiency in utilizing visible light and can promote photoelectron transfer.

The initial pH of the solution containing the persistent pollutants was adjusted with 1 M hydrochloric acid. Figure 5c,d shows that both the degradation effect and the adsorption effect decreased significantly at pH = 2 and pH = 4. The possible reason for this is that the structure of the hollow nanocatalyst may be damaged under strongly acidic conditions, thus affecting the degradation in the pollutants. The reported performance of the photocatalysts

applied for the degradation in TC and 2-CP is presented in Tables 1 and 2. Compared with the photocatalyst materials listed in the tables, it reveals that the $Zn_{1-x}Cd_xS$ catalyst synthesized herein has excellent visible light catalytic activity for the degradation in TC and 2-CP organic pollutants.

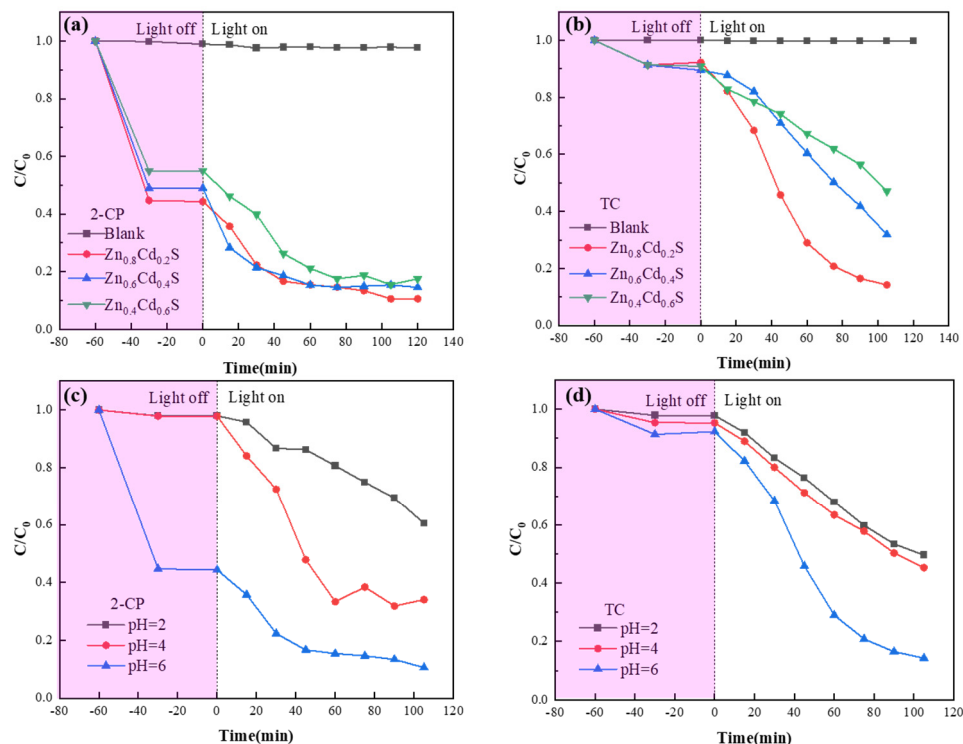


Figure 5. Photocatalytic removal curves under visible light irradiation. (a) Degradation in 2-CP; (b) Degradation in TC; (c) Degradation in 2-CP, HCl adjust Ph; (d) Degradation in 2-CP, HCl adjust pH.

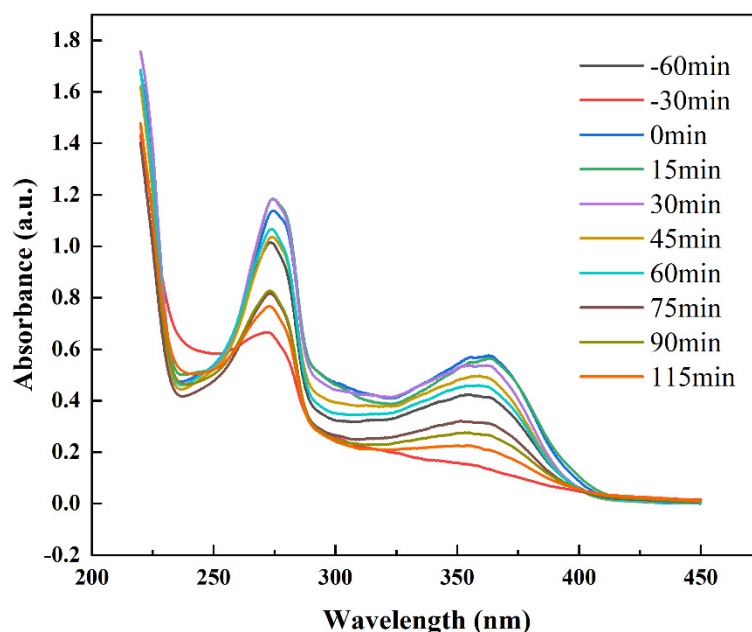
Table 1. Comparison of the performance of different photocatalysts for TC degradation.

Photocatalysts	Concentration of Catalyst (g/L)	Concentration of TC (mg/L)	Light Source	Irradiation Time (h)	Degradation Rate (%)	Reference
$Zn_{1-x}Cd_xS$	0.5	50	300 W Xenon lamp (>400 nm)	2	91	This work
ZnO_2	0.1	50	300 W Xenon lamp (>400 nm)	4	83.7	[38]
$BiOBr/MnFe_2O_4$	1	20	simulated sunlight lamp	1.5	76.5	[39]
$BiOCl@CeO_2$	0.5	10	300 W Xenon lamp (>400 nm)	2	92	[40]
$Ag-ZnS/rGO$	1.25	10	300 W Xenon lamp (>400 nm)	2	90	[41]
N-ZnS	0.3	10	300 W Xenon lamp (>400 nm)	2.5	90	[42]
$BiOCl/CdS$	6	10	300 W Xenon lamp (>400 nm)	1.7	93	[43]

The two contaminants were added to the aqueous solution simultaneously at the same levels as when the experiments were conducted separately, and the aqueous solution was scanned at full wavelength using a UV-Vis spectrometer. As shown in Figure 6, the levels of both pollutants in the aqueous solution showed a decreasing trend with time after the light was switched on. This indicates that the $Zn_{1-x}Cd_xS$ catalyst showed a superior removal efficiency for TC when both persistent pollutants were present in the aqueous solution at the same time.

Table 2. Comparison of the performance of different photocatalysts for the degradation in 2-CP.

Photocatalysts	Concentration of Catalyst (g/L)	Concentration of 2-CP (mg/L)	Light Source	Irradiation Time (h)	Degradation Rate (%)	Reference
Zn _{1-x} Cd _x S	0.5	50	300W Xenon lamp (>400 nm)	2	90	This work
WO ₃ /WS ₂ /PANI	0.5	35	300 W Xenon lamp (>400 nm)	3	91	[44]
CuO-GO/TiO ₂	0.5	10	104W cool white lamp	3.5	85	[45]
B/N-graphene-coated Cu/TiO ₂	0.25	5	1000W Xenon lamp (<550 nm)	1.3	92	[46]
SiO ₂ /ZrO ₂	0.375	10	400W metal halide lamp (>400 nm)	4	92	[47]

**Figure 6.** UV-spectra of TC and 2-CP degradation over time on stream.

2.3. Kinetic Studies

Both pollutants were optimally degraded when the initial pH of the solution = 6, and the catalysts showed the best photocatalytic performance for each pollutant. Under such optimum initial conditions, a linear fit was performed for the removal of the persistent pollutants from the solution, as shown in Figure 7a,b, and the results of the fit were consistent with a pseudo-first order kinetic model. For both contaminants, a 20% Cd doping rate resulted in a maximum degradation rate of 0.03706 min^{-1} for 2-CP and 0.00776 min^{-1} for TC. As shown in Figure 7c,d, when a 1M hydrochloric acid solution was used to adjust the initial pH of the solution, the fitted results were consistent with the pseudo-first order kinetic model, with the maximum degradation rate at pH = 6 when on Zn_{0.8}Cd_{0.2}S.

2.4. Effect of Temperature

The reaction temperature was screened under the basis of the optimum degradation conditions listed in Section 3.2. As shown in Figure 8, the photocatalyst Zn_{1-x}Cd_xS showed a decreasing trend in the degradation in both organic pollutants with increasing temperature at a dosage of 50 mg and pH = 6. This may be due to the fact that the dissolved oxygen in the organic pollutant solution declines as the temperature increases, resulting in a downward concentration of superoxide radicals leading to a decrease in the degradation performance of the pollutants [48].

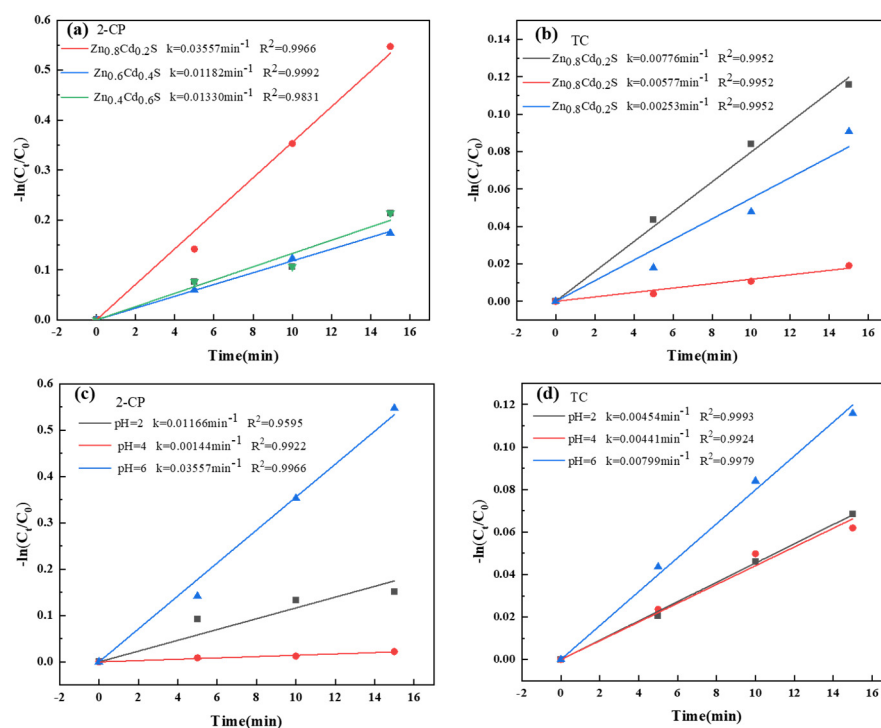


Figure 7. The Kinetic fitting curves. (a) The Kinetic fittings of 2-CP. (b) The Kinetic fittings of TC. (c) The Kinetic fittings of 2-CP, HCl adjust pH. (d) The Kinetic fittings of TC, HCl adjust pH.

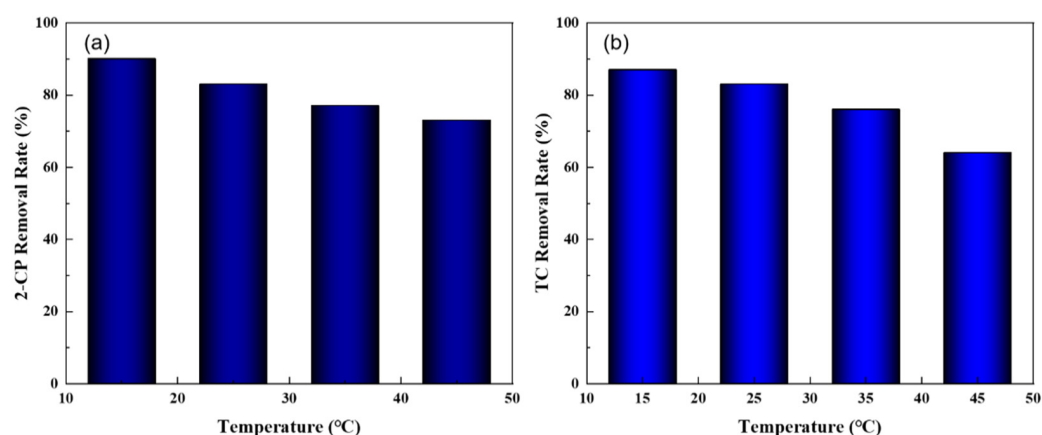


Figure 8. (a) Effect of temperature on the degradation in organic pollutant 2-CP (b) Effect of temperature on the degradation in organic pollutant TC.

2.5. Photoelectrochemical Analysis

The transient photocurrent test of the catalyst sample allows the study of the broadband response of the catalyst. It can be seen from Figure 9 that the current intensity changes significantly at the moment the light is turned on. The strong photocurrent indicates that the doping of Cd promotes the carrier transfer and separation, and the strong current intensity of $Zn_{1-x}Cd_xS$ is due to the change of band gap width by the doping of Cd, which improves the utilization of visible light.

2.6. Degradation Properties of $Zn_{1-x}Cd_xS$ -Activated PMS

The optimum photocatalyst $Zn_{0.8}Cd_{0.2}S$ was selected based on the results of the previous experiments to investigate the degradation in TC and 2-CP with different PMS dosages. In this section, different concentrations of PMS were set up for the degradation in TC and 2-CP. As shown in Figure 10a, b, the degradation efficiency of 2-CP increased

from 79% to 90% with the increase in PMS dosage, and the best degradation effect and the maximum reaction rate were achieved when the PMS dosage was 0.02 mM. The degradation efficiency of 2-CP increased from 79% to 90%, and the best degradation effect and maximum reaction rate was achieved at 0.02 mM PMS. According to Figure 10c,d, the degradation efficiency of TC increased and then decreased with increasing PMS dosage, and the best degradation effect was achieved at 0.02 mM. The graph shows that when the dosage is more than 0.02 mM, the degradation process is more obviously inhibited. This may be due to the fact that the excess amount of PMS obstructs other types of reactive oxygen radicals (ROS) from generating. As the amount of photocatalyst is constant and therefore the amount of PMS that can be activated is constant, an excess of PMS may not be activated and may cause an increase in turbidity in the solution, thus preventing light from reaching the solution, resulting in poor light utilization [49].

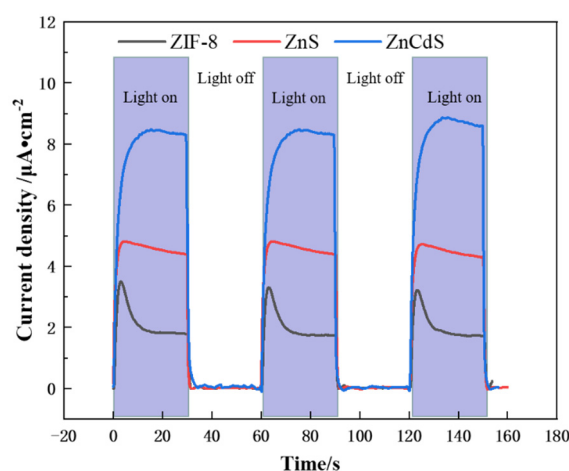


Figure 9. Transient photocurrent responses of catalysts.

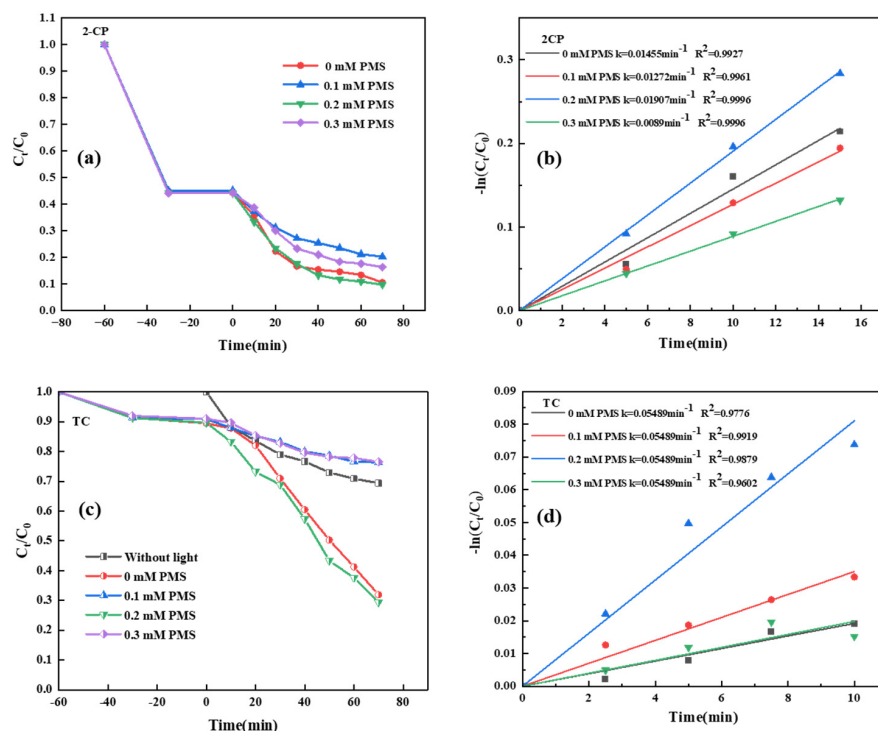


Figure 10. Photocatalytic contaminant removal curves and kinetic fitting curves for ZIF-8 activated PMS. (a) Degradation and (b) The kinetic fittings of 2-CP. (c) Degradation and (d) The kinetic fittings of TC.

2.7. Possible Photocatalytic Mechanism

The capture experiments can help to understand the main active species in the photocatalytic degradation process. The scavengers added to the solution containing persistent pollutants were isopropyl alcohol, p-benzoquinone and EDTA-2Na to capture hydroxyl radicals ($\bullet\text{OH}$), superoxide radicals ($\bullet\text{O}_2^-$) and vacancies (h^+), respectively. The addition of BQ to the solution containing TC and to the solution containing 2-CP, respectively, greatly reduced the degradation rate of both contaminants. The addition of IPA and EDTA-2Na to the solution containing contaminants did not significantly hinder the degradation effect. Thus, the experiments can prove that superoxide radicals are the main active species for the degradation in TC and 2-CP (Figure 11).

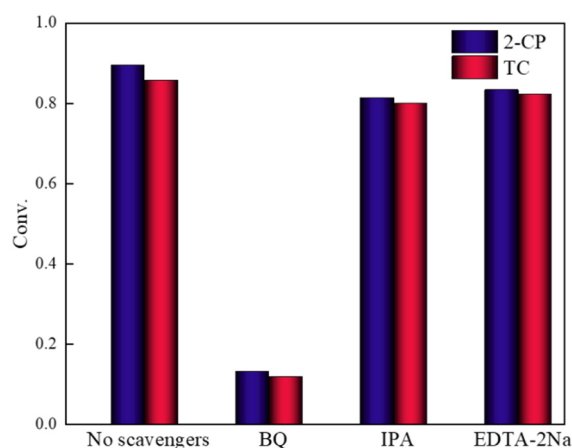


Figure 11. Scavenger experiments.

$\bullet\text{O}_2^-$, $\bullet\text{OH}$, h^+ are the main reactive oxygen radicals during the mineralization of TC molecules and 2-CP molecules. During the course of the experiment, the organic pollutant molecules are first adsorbed on the surface of the catalyst and when the light starts, the electrons are first excited from the valence band to the conduction band. O_2 continues to be adsorbed on the surface, forming O_2^- with electrons, which is then further reduced to H_2O_2 and $-\text{OH}$. In addition, the h^+ accumulated on the VB can also be used for the degradation in pollutant molecules as seen in Figure 12. The $\bullet\text{O}_2^-$ play a major role in the degradation of organic pollutants throughout the photocatalytic reaction process. In contrast, h^+ and $\bullet\text{OH}$ play an auxiliary role in the degradation in organic pollutants. The introduction of Cd^{2+} enhances the light absorption, accelerates charge separation and transfer, enhances the adsorption of oxygen and produces more highly active substances, which is conducive to enhancing the activity of photocatalytic degradation in organic pollutants.

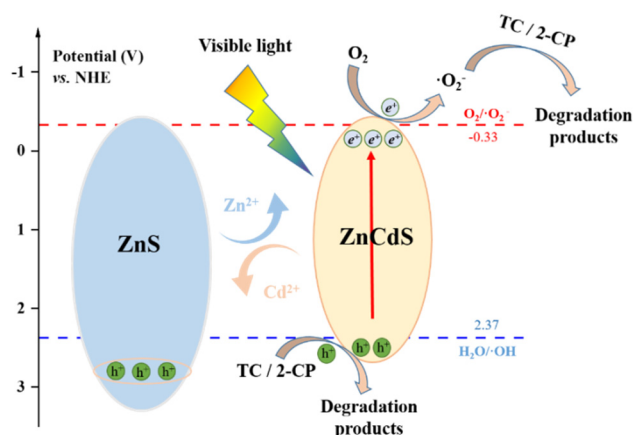
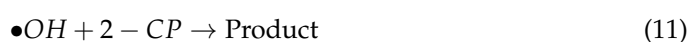
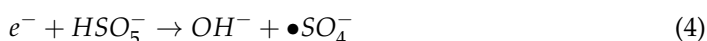
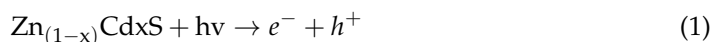


Figure 12. Possible photocatalytic mechanism of photocatalytic TC degradation and 2-CP degradation.

From this, we propose a possible photocatalytic reaction, which is as follows:



2.8. Photocatalyst Stability Testing

To investigate the stability of the optimized catalyst, the photocatalyst material synthesized for the degradation in persistent pollutants was recovered from solution, washed three times with anhydrous ethanol and deionized water and then dried in an oven, and will be repeated for photocatalytic degradation experiments. Figure 13a,b show the stability and recoverability of the photocatalysts implanted. The photocatalytic experiments were repeated three times en route and there was no significant change in the degradation efficiency for the pollutants (TC and 2-CP). This indicates that under suitable conditions, the prepared photocatalysts are highly stable and can be repeated for photocatalytic degradation experiments, which is particularly important in the field of photocatalytic removal of contaminants from aqueous solutions.

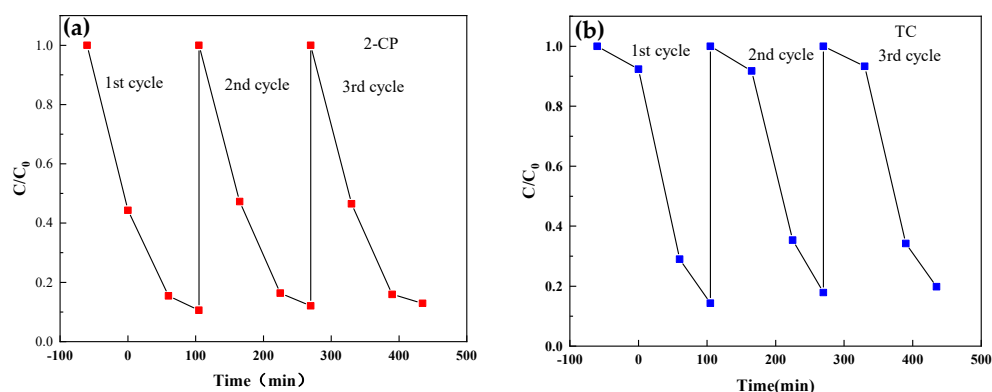


Figure 13. Photo-stability and recyclability of the optimized catalyst. (a) Application to 2-CP degradability reusability trials. (b) Application to TC degradability reusability trials.

3. Materials and Method

3.1. Chemicals

Zinc acetate dihydrate ($\text{Zn}(\text{CH}_3\text{COO})_2 \cdot 2\text{H}_2\text{O}$, AR), Cadmium acetate dehydrate ($\text{Cd}(\text{CH}_3\text{COO})_2 \cdot 2\text{H}_2\text{O}$, AR), 2-Chlorophenol (2-CP, 99%), Tetracycline hydrochloride (TC, 99%), thioacetamide (TAA, 98%), Ammonium persulfate ($(\text{NH}_4)_2\text{S}_2\text{O}_8$, AR), 1-methylimidazole (98%) and 2-methylimidazole (98%, $\text{C}_4\text{H}_6\text{N}_2$) were purchased from Aladdin Industries

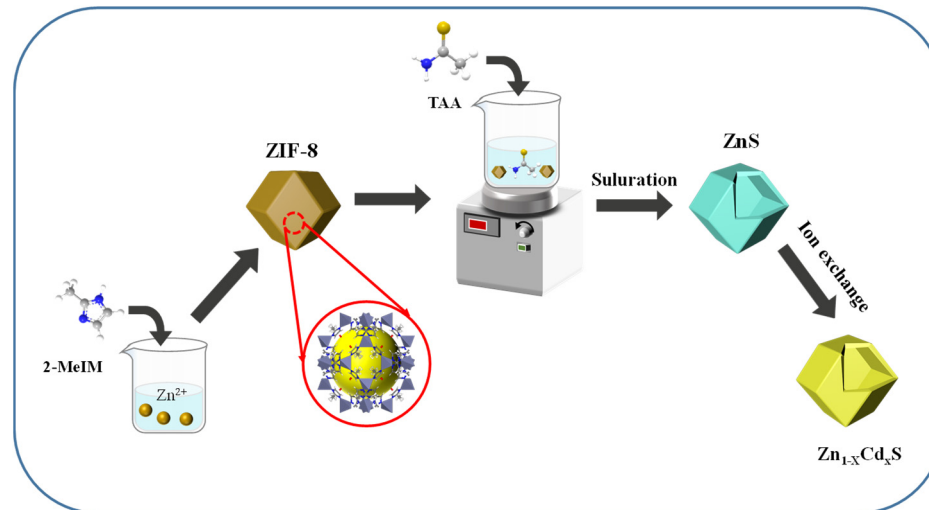
(Shanghai, China). Methanol (AR), ethanol (AR), ethanediol (AR), p-benzoquinone (BQ), isopropanol (IPA, AR), EDTA-2Na were purchased from Sinopharm Chemical Reagent (Shanghai, China). All of the materials were used without further purification.

3.2. Synthesis of ZIF-8

ZIF-8 was synthesized by improving on the previously reported synthesis method [50,51]. $\text{Zn}(\text{CH}_3\text{COO})_2 \cdot 2\text{H}_2\text{O}$ and 1-methylimidazole, 2-methylimidazole were dissolved in 20 mL of anhydrous methanol, sonicated until completely dissolved, then noted as solution A and B, respectively. Solution A was poured into solution B with rapid stirring to mix thoroughly and stirred slowly at room temperature for 24 h. The white solid obtained by centrifugation was washed three times with anhydrous ethanol and dried overnight in a drying oven at 60 °C.

3.3. Synthesis of $\text{Zn}_{1-x}\text{Cd}_x\text{S}$ Nanocages

$\text{Zn}_{1-x}\text{Cd}_x\text{S}$ nanocages are synthesized by improving on the previous work [52]. ZIF-8 was dissolved in 40 mL of anhydrous methanol and 500 mg of thioacetamide (TAA) was dissolved in 10 mL of anhydrous ethanol and stirred separately until completely dissolved. The two liquids were mixed and stirred slowly and continuously at 50 °C for 24 h. A certain amount of $\text{Cd}(\text{CH}_3\text{COO})_2 \cdot 2\text{H}_2\text{O}$ was taken and dissolved in ethylene glycol to dissolve completely. The above two solutions were mixed and stirred for 30 min and then transferred to a 100 mL PTFE-lined hydrothermal reactor and kept at 160 °C for 4 h. The resulting samples were separated by centrifugation, washed three times with anhydrous ethanol and dried in a drying oven at 60 °C overnight. The amount of $\text{Cd}(\text{CH}_3\text{COO})_2 \cdot 2\text{H}_2\text{O}$ was added to obtain different $\text{Zn}_{1-x}\text{Cd}_x\text{S}$ catalysts ($x = 0.2, 0.4$ and 0.6). The preparation process is shown in Scheme 1.



Scheme 1. Schematic diagram of hollow $\text{Zn}_{1-x}\text{Cd}_x\text{S}$ nanocage preparation.

3.4. Photocatalytic Activity Measurements

2-chlorophenol (2-CP) and tetracycline hydrochloride (TC) were selected as organic pollutants. The photocatalytic degradation experiments were carried out in a 100 mL reaction vessel containing 100 mL of the organic pollutant solution (50 mg/L of 2-CP or 40 mg/L of TC). After adding 50 mg of photocatalyst to the organic contaminant solution and stirring for 30 min in the dark until adsorption–desorption equilibrium, the contaminants were irradiated with visible light at a cut-off wavelength of 420 nm using a 300 W xenon lamp (Magnesium Rixon MC-PF300, Beijing, China). Samples were taken at 15 min intervals and filtered through a 0.45 μm filter to remove catalyst particles from the solution, and the absorbance of 2-chlorophenol and tetracycline hydrochloride were

measured at 274 nm and 356 nm, respectively, using a UV spectrophotometer (PERSEE, TU-1950, Beijing, China), with the method of scanning from 200 nm to 450 nm.

The photocatalytic degradation efficiency can be calculated by Equation (13), and C_0 and C_t denote the initial concentration of the pollutant and the concentration after a reaction period, respectively.

$$\text{Degradation rate : } D\% = \frac{C_0 - C_t}{C_0} \times 100\% \quad (13)$$

3.5. PMS Activation Photocatalytic Reaction Test

For photocatalytic reactions using PMS activation, 50 mg of catalyst samples were added to the reactor (100 mL, 50 mg/L of 2-CP or 40 mg/L of TC), stirred for 0.5 h in the dark to reach adsorption–desorption equilibrium, and then 0.01 mM, 0.02 mM and 0.3 mM PMS oxidants were added to the reactor. A sample of 4 mL was taken at 15 min intervals and the catalyst was separated from the solution using a 0.45 μm needle filter and tested as in 2.4 above.

3.6. Free radical Capture Test

Under the same conditions as the photocatalytic degradation in pollutants, p-benzoquinone (BQ), isopropanol (IPA), and EDTA-2Na were used as trapping agents for superoxide radicals ($\bullet\text{O}_2^-$), hydroxyl radicals ($\bullet\text{OH}$), and holes (h^+). For the cycling experiments of photocatalysts, the photocatalysts were centrifuged and washed with deionized water and continued to be used for photocatalytic degradation cycle experiments.

3.7. Electrochemical Testing

Photocurrent tests were performed on an electrochemical workstation with a standard triple electrode. The electrolyte was 0.5 M H_2SO_4 , the counter electrode was a platinum wire, the reference electrode was an Ag/AgCl electrode, and the working electrode was a catalyst sample coated on an ITO electrode. The working electrode was prepared by taking 5 mg of sample dissolved in 150 μL of anhydrous ethanol, adding 15 μL of naphthol to the solution and sonicating. The sonication finished solution was coated on the ITO glass with an area of 10 mm \times 15 mm and the coating area was 10 mm \times 10 mm.

4. Conclusions

In summary, $\text{Zn}_{1-x}\text{Cd}_x\text{S}$ is excellent for the degradation in pollutants under UV-Vis conditions, but has a limiting effect on pH adjustment. When the pH was close to neutral, the catalyst showed good adsorption and photocatalytic degradation, achieving over 90% removal of the pollutant within 120 min. At the same time, some inhibition of the photocatalytic process occurs with increasing temperature. In photocurrent response tests it was shown that the doping of Cd broadened the absorption of light and had a higher migration rate of electrons. It was shown that $\bullet\text{O}_2^-$ was the main reactive radical. We therefore propose a possible electron transfer mechanism and reaction mechanism. $\text{Zn}_{1-x}\text{Cd}_x\text{S}$ also has a certain activation ability for PMS and shows a certain promotion effect for the removal of organic pollutants when PMS is dosed at 0.02 mM in solutions containing organic pollutants.

Author Contributions: J.T.: Conceptualization, Investigation, Data curation, Writing—original draft; G.W.: Validation, Data curation; Z.W.: Validation, Data curation; H.S.: Validation, Data curation; L.L.: Investigation, Validation; C.L.: Supervision, Validation, Writing—review and editing; J.B.: Methodology, Supervision, Writing—review and editing. All authors have read and agreed to the published version of the manuscript.

Funding: This research is funded by the 2021 China Ministry of Education University-Industry Collaborative Education Project under grant number KGRCYJY2021011.

Conflicts of Interest: The authors declare no conflict of interest.

References

1. Xu, R.; Yang, Z.-H.; Wang, Q.-P.; Bai, Y.; Liu, J.-B.; Zheng, Y.; Zhang, Y.-R.; Xiong, W.-P.; Ahmad, K.; Fan, C.-Z. Rapid startup of thermophilic anaerobic digester to remove tetracycline and sulfonamides resistance genes from sewage sludge. *Sci. Total Environ.* **2018**, *612*, 788–798. [[CrossRef](#)]
2. Tozar, T.; Boni, M.; Staicu, A.; Pascu, M.L. Optical Characterization of Ciprofloxacin Photolytic Degradation by UV-Pulsed Laser Radiation. *Molecules* **2021**, *26*, 2324. [[CrossRef](#)]
3. Liu, X.; Huang, L.; Wu, X.; Wang, Z.; Dong, G.; Wang, C.; Liu, Y.; Wang, L. Bi₂Zr₂O₇ nanoparticles synthesized by soft-templated sol-gel methods for visible-light-driven catalytic degradation of tetracycline. *Chemosphere* **2018**, *210*, 424–432. [[CrossRef](#)]
4. Sun, S.; Wang, Y.; Zhou, L.; Wang, X.; Kang, C. Enhanced degradation mechanism of tetracycline by MnO₂ with the presence of organic acids. *Chemosphere* **2022**, *286*, 131606. [[CrossRef](#)]
5. Wang, X.; Zhu, G.; Wang, C.; Niu, Y. Effective degradation of tetracycline by organic-inorganic hybrid materials induced by triethylenediamine. *Environ. Res.* **2021**, *198*, 111253. [[CrossRef](#)]
6. Zhang, Q.; Xu, J.; Ma, X.; Xu, J.; Yun, Z.; Zuo, Q.; Wang, L. A novel Fe-based bi-MOFs material for photocatalytic degradation of tetracycline: Performance, mechanism and toxicity assessment. *J. Water Process Eng.* **2021**, *44*, 102364. [[CrossRef](#)]
7. Channei, D.; Nakaruk, A.; Khanitchaidecha, W.; Jannoey, P.; Phanichphant, S. Hybrid high-porosity rice straw infused with BiVO₄ nanoparticles for efficient 2-chlorophenol degradation. *Int. J. Appl. Ceram. Technol.* **2019**, *16*, 1060–1068. [[CrossRef](#)]
8. Yasmeen, H.; Zada, A.; Ali, S.; Khan, I.; Ali, W.; Khan, W.; Khan, M.; Anwar, N.; Ali, A.; Huerta-Flores, A.M.; et al. Visible light-excited surface plasmon resonance charge transfer significantly improves the photocatalytic activities of ZnO semiconductor for pollutants degradation. *J. Chin. Chem. Soc.* **2020**, *67*, 1611–1617. [[CrossRef](#)]
9. Wu, S.; Hu, H.; Lin, Y.; Zhang, J.; Hu, Y.H. Visible light photocatalytic degradation of tetracycline over TiO₂. *Chem. Eng. J.* **2020**, *382*, 122842. [[CrossRef](#)]
10. Lim, S.J.; Kim, T.-H. Combined treatment of swine wastewater by electron beam irradiation and ion-exchange biological reactor system. *Sep. Purif. Technol.* **2015**, *146*, 42–49. [[CrossRef](#)]
11. Shu, J.; Wang, Z.; Huang, Y.; Huang, N.; Ren, C.; Zhang, W. Adsorption removal of Congo red from aqueous solution by polyhedral Cu₂O nanoparticles: Kinetics, isotherms, thermodynamics and mechanism analysis. *J. Alloys Compd.* **2015**, *633*, 338–346. [[CrossRef](#)]
12. Lei, C.; Zhu, X.; Zhu, B.; Jiang, C.; Le, Y.; Yu, J. Superb adsorption capacity of hierarchical calcined Ni/Mg/Al layered double hydroxides for Congo red and Cr(VI) ions. *J. Hazard. Mater.* **2017**, *321*, 801–811. [[CrossRef](#)] [[PubMed](#)]
13. Wang, H.; Wu, Y.; Feng, M.; Tu, W.; Xiao, T.; Xiong, T.; Ang, H.; Yuan, X.; Chew, J.W. Visible-light-driven removal of tetracycline antibiotics and reclamation of hydrogen energy from natural water matrices and wastewater by polymeric carbon nitride foam. *Water Res.* **2018**, *144*, 215–225. [[CrossRef](#)] [[PubMed](#)]
14. Cabrera-Reina, A.; Martínez-Piernas, A.B.; Bertakis, Y.; Xekoukoulotakis, N.P.; Agüera, A.; Sánchez Pérez, J.A. TiO₂ photocatalysis under natural solar radiation for the degradation of the carbapenem antibiotics imipenem and meropenem in aqueous solutions at pilot plant scale. *Water Res.* **2019**, *166*, 115037. [[CrossRef](#)]
15. Li, C.-J.; Zhao, R.; Peng, M.-Q.; Gong, X.-L.; Xia, M.; Li, K.; Huang, Z.-B.; Xia, D.-S. Mechanism study on denitration by new PMS modified bamboo charcoal bifunctional photocatalyst. *Chem. Eng. J.* **2017**, *316*, 544–552. [[CrossRef](#)]
16. Oh, W.-D.; Ng, C.-Z.; Ng, S.-L.; Lim, J.-W.; Leong, K.-H. Rapid degradation of organics by peroxymonosulfate activated with ferric ions embedded in graphitic carbon nitride. *Sep. Purif. Technol.* **2020**, *230*, 115852. [[CrossRef](#)]
17. Shao, H.; Zhao, X.; Wang, Y.; Mao, R.; Wang, Y.; Qiao, M.; Zhao, S.; Zhu, Y. Synergetic activation of peroxymonosulfate by Co₃O₄ modified g-C₃N₄ for enhanced degradation of diclofenac sodium under visible light irradiation. *Appl. Catal. B Environ.* **2017**, *218*, 810–818. [[CrossRef](#)]
18. Gong, Y.; Zhao, X.; Zhang, H.; Yang, B.; Xiao, K.; Guo, T.; Zhang, J.; Shao, H.; Wang, Y.; Yu, G. MOF-derived nitrogen doped carbon modified g-C₃N₄ heterostructure composite with enhanced photocatalytic activity for bisphenol A degradation with peroxymonosulfate under visible light irradiation. *Appl. Catal. B Environ.* **2018**, *233*, 35–45. [[CrossRef](#)]
19. Feng, C.; Chen, Z.; Jing, J.; Sun, M.; Tong, H.; Hou, J. Band structure and enhanced photocatalytic degradation performance of Mg-doped CdS nanorods. *Phys. B Condens. Matter* **2020**, *594*, 412363. [[CrossRef](#)]
20. Yan, S.C.; Li, Z.S.; Zou, Z.G. Photodegradation Performance of g-C₃N₄ Fabricated by Directly Heating Melamine. *Langmuir* **2009**, *25*, 10397–10401. [[CrossRef](#)]
21. Bo, T.; Wang, Y.; Wang, J.; Zhao, Z.; Zhang, J.; Zheng, K.; Lin, T.; Zhang, B.; Shao, L. Photocatalytic H₂ evolution on CdS modified with partially crystallized MoS₂ under visible light irradiation. *Chem. Phys. Lett.* **2020**, *746*, 137305. [[CrossRef](#)]
22. Su, J.; Yu, S.; Xu, M.; Guo, Y.; Sun, X.; Fan, Y.; Zhang, Z.; Yan, J.; Zhao, W. Enhanced visible light photocatalytic performances of few-layer MoS₂@TiO₂ hollow spheres heterostructures. *Mater. Res. Bull.* **2020**, *130*, 110936. [[CrossRef](#)]
23. Ethiraj, A.S.; Hebalkar, N.; Sainkar, S.R.; Urban, J.; Kulkarni, S.K. Synthesis and Investigation of ZnS Nanoparticles Adsorbed On Functionalised Silica Particles. *Surf. Eng.* **2004**, *20*, 367–372. [[CrossRef](#)]
24. Mahajan, J.; Jeevanandam, P. A facile thermal decomposition approach for the synthesis of SiO₂@ZnS core-shell nanoparticles and their application as effective adsorbent for the removal of congo red. *Mater. Today Commun.* **2021**, *26*, 102085. [[CrossRef](#)]

25. Guo, J.; Khan, S.; Cho, S.-H.; Kim, J. ZnS nanoparticles as new additive for polyethersulfone membrane in humic acid filtration. *J. Ind. Eng. Chem.* **2019**, *79*, 71–78. [[CrossRef](#)]
26. Ruan, D.; Fujitsuka, M.; Majima, T. Exfoliated Mo₂C nanosheets hybridized on CdS with fast electron transfer for efficient photocatalytic H₂ production under visible light irradiation. *Appl. Catal. B Environ.* **2020**, *264*, 118541. [[CrossRef](#)]
27. Zhong, W.; Wu, X.; Wang, P.; Fan, J.; Yu, H. Homojunction CdS Photocatalysts with a Massive S₂—Adsorbed Surface Phase: One-Step Facile Synthesis and High H₂-Evolution Performance. *ACS Sustain. Chem. Eng.* **2020**, *8*, 543–551. [[CrossRef](#)]
28. Reddy, C.V.; Shim, J.; Cho, M. Synthesis, structural, optical and photocatalytic properties of CdS/ZnS core/shell nanoparticles. *J. Phys. Chem. Solids* **2017**, *103*, 209–217. [[CrossRef](#)]
29. Liu, M.; Wang, L.; Lu, G.; Yao, X.; Guo, L. Twins in Cd_{1-x}Zn_xS solid solution: Highly efficient photocatalyst for hydrogen generation from water. *Energy Environ. Sci.* **2011**, *4*, 1372–1378. [[CrossRef](#)]
30. Wang, D.; Li, Z. Iron-based metal–organic frameworks (MOFs) for visible-light-induced photocatalysis. *Res. Chem. Intermed.* **2017**, *43*, 5169–5186. [[CrossRef](#)]
31. Zhang, X.; Wang, J.; Dong, X.-X.; Lv, Y.-K. Functionalized metal-organic frameworks for photocatalytic degradation of organic pollutants in environment. *Chemosphere* **2020**, *242*, 125144. [[CrossRef](#)] [[PubMed](#)]
32. Jiang, W.; Li, Z.; Liu, C.; Wang, D.; Yan, G.; Liu, B.; Che, G. Enhanced visible-light-induced photocatalytic degradation of tetracycline using BiOI/MIL-125(Ti) composite photocatalyst. *J. Alloys Compd.* **2021**, *854*, 157166. [[CrossRef](#)]
33. Chen, J.; Chen, J.; Li, Y. Hollow ZnCdS dodecahedral cages for highly efficient visible-light-driven hydrogen generation. *J. Mater. Chem. A* **2017**, *5*, 24116–24125. [[CrossRef](#)]
34. Bai, T.; Shi, X.; Liu, M.; Huang, H.; Yu, M.-H.; Zhang, J.; Bu, X.-H. A metal–organic framework-derived Zn_{1-x}Cd_xS/CdS heterojunction for efficient visible light-driven photocatalytic hydrogen production. *Dalton Trans.* **2021**, *50*, 6064–6070. [[CrossRef](#)] [[PubMed](#)]
35. Wu, L.; Fu, H.; Wei, Q.; Zhao, Q.; Wang, P.; Wang, C.-C. Porous Cd_{0.5}Zn_{0.5}S nanocages derived from ZIF-8: Boosted photocatalytic performances under LED-visible light. *Environ. Sci. Pollut. Res.* **2021**, *28*, 5218–5230. [[CrossRef](#)] [[PubMed](#)]
36. Song, H.; Wang, N.; Meng, H.; Han, Y.; Wu, J.; Xu, J.; Xu, Y.; Zhang, X.; Sun, T. A facile synthesis of a ZIF-derived ZnS/ZnIn₂S₄ heterojunction and enhanced photocatalytic hydrogen evolution. *Dalton Trans.* **2020**, *49*, 10816–10823. [[CrossRef](#)]
37. Luca, V.; Djajanti, S.; Howe, R.F. Structural and Electronic Properties of Sol–Gel Titanium Oxides Studied by X-ray Absorption Spectroscopy. *J. Phys. Chem. B* **1998**, *102*, 10650–10657. [[CrossRef](#)]
38. Chen, P.; Dong, N.; Zhang, J.; Wang, W.; Tan, F.; Wang, X.; Qiao, X.; Keung Wong, P. Investigation on visible-light photocatalytic performance and mechanism of zinc peroxide for tetracycline degradation and Escherichia coli inactivation. *J. Colloid Interface Sci.* **2022**, *624*, 137–149. [[CrossRef](#)]
39. He, Q.; Ge, M. Visible-light activation of peroxydisulfate by magnetic BiOBr/MnFe₂O₄ nanocomposite toward degradation of tetracycline. *J. Mater. Sci. Mater. Electron.* **2022**, *33*, 5859–5877. [[CrossRef](#)]
40. Wang, H.; Liao, B.; Lu, T.; Ai, Y.; Liu, G. Enhanced visible-light photocatalytic degradation of tetracycline by a novel hollow BiOCl@CeO₂ heterostructured microspheres: Structural characterization and reaction mechanism. *J. Hazard. Mater.* **2020**, *385*, 121552. [[CrossRef](#)]
41. Kameli, S.; Mehrizad, A. Ultrasound-assisted Synthesis of Ag-ZnS/rGO and its Utilization in Photocatalytic Degradation of Tetracycline Under Visible Light Irradiation. *Photochem. Photobiol.* **2019**, *95*, 512–521. [[CrossRef](#)] [[PubMed](#)]
42. Zhu, B.; Jiang, G.; Kong, C.; Sun, J.; Liu, F.; Wang, Y.; Zhao, C.; Liu, C. Photocatalytic degradation of organic pollutants in water by N-doping ZnS with Zn vacancy: Enhancement mechanism of visible light response and electron flow promotion. *Environ. Sci. Pollut. Res.* **2022**, *29*, 58716–58729. [[CrossRef](#)] [[PubMed](#)]
43. Yang, L.; Wang, J.; Zhang, Y.; Zhou, B.; Tan, P.; Pan, J. Construction of S-scheme BiOCl/CdS composite for enhanced photocatalytic degradation of antibiotic. *J. Mater. Sci. Mater. Electron.* **2022**, *33*, 13303–13315. [[CrossRef](#)]
44. Barakat, M.A.; Kumar, R.; Almeelbi, T.; Al-Mur, B.A.; Eniola, J.O. Sustainable visible light photocatalytic scavenging of the noxious organic pollutant using recyclable and reusable polyaniline coupled WO₃/WS₂ nanohybrid. *J. Clean. Prod.* **2022**, *330*, 129942. [[CrossRef](#)]
45. Alafif, Z.O.; Anjum, M.; Kumar, R.; Abdelbasir, S.M.; Barakat, M.A. Synthesis of CuO–GO/TiO₂ visible light photocatalyst for 2-chlorophenol degradation, pretreatment of dairy wastewater and aerobic digestion. *Appl. Nanosci.* **2019**, *9*, 579–591. [[CrossRef](#)]
46. Ombaka, L.M.; McGettrick, J.D.; Oseghe, E.O.; Al-Madanat, O.; Rieck genannt Best, F.; Msagati, T.A.M.; Davies, M.L.; Bredow, T.; Bahnemann, D.W. Photocatalytic H₂ production and degradation of aqueous 2-chlorophenol over B/N-graphene-coated CuO/TiO₂: A DFT, experimental and mechanistic investigation. *J. Environ. Manag.* **2022**, *311*, 114822. [[CrossRef](#)]
47. Hassan, N.S.; Jalil, A.A.; Aziz, F.F.A.; Fauzi, A.A.; Azami, M.S.; Jusoh, N.W.C. Tailoring the Silica Amount in Stabilizing the Tetragonal Phase of Zirconia for Enhanced Photodegradation of 2-Chlorophenol. *Top. Catal.* **2020**, *63*, 1145–1156. [[CrossRef](#)]
48. Saadati, F.; Keramati, N.; Ghazi, M.M. Influence of parameters on the photocatalytic degradation of tetracycline in wastewater: A review. *Crit. Rev. Environ. Sci. Technol.* **2016**, *46*, 757–782. [[CrossRef](#)]
49. Ji, Q.; Cheng, X.; Wu, Y.; Xiang, W.; He, H.; Xu, Z.; Xu, C.; Qi, C.; Li, S.; Zhang, L.; et al. Visible light absorption by perylene diimide for synergistic persulfate activation towards efficient photodegradation of bisphenol A. *Appl. Catal. B Environ.* **2021**, *282*, 119579. [[CrossRef](#)]

50. Jiang, Z.; Sun, H.; Qin, Z.; Jiao, X.; Chen, D. Synthesis of novel ZnS nanocages utilizing ZIF-8 polyhedral template. *Chem. Commun.* **2012**, *48*, 3620–3622. [[CrossRef](#)]
51. Zhan, W.-w.; Kuang, Q.; Zhou, J.-z.; Kong, X.-j.; Xie, Z.-x.; Zheng, L.-s. Semiconductor@Metal–Organic Framework Core–Shell Heterostructures: A Case of ZnO@ZIF-8 Nanorods with Selective Photoelectrochemical Response. *J. Am. Chem. Soc.* **2013**, *135*, 1926–1933. [[CrossRef](#)] [[PubMed](#)]
52. Qiu, B.; Zhu, Q.; Xing, M.; Zhang, J. A robust and efficient catalyst of $Cd_xZn_{1-x}Se$ motivated by CoP for photocatalytic hydrogen evolution under sunlight irradiation. *Chem. Commun.* **2017**, *53*, 897–900. [[CrossRef](#)] [[PubMed](#)]